Discover Sustainability

Research

Polystyrene infused with functionalized reduced graphene oxide as a reusable oil sorbent

Isaiah Olufemi Akanji[1,2] · Samuel Ayodele Iwarere[3] · Badruddeen Saulawa Sani[4] · Bello Mukhtar[1] · Baba El-Yakubu Jibril[1] · Michael Olawale Daramola[3]

Received: 17 July 2024 / Accepted: 1 August 2024
Published online: 21 August 2024

Abstract
Adsorption has been reported to be optimal among oil spill cleanup methods due to its simplicity, low capital and operational cost, high removal efficiency and environmental friendliness. However, its continuous usage has been linked to generation of enormous waste, after oil spill cleanup, to which use of reusable oil sorbents has been proposed as a possible solution. Synthetic organic oil sorbents have high mechanical properties compared to other categories of oil sorbents, but they suffer low adsorptive capacities. To address this problem, among other nanoparticles, rGO have been infused in polymeric materials to produce composite oil sorbents characterized with high adsorptive capacities. In this research, surface modified rGO was infused in waste expanded polystyrene, to produce electrospun PS/FrGO composite sorbents by solution blending and electrospinning method. Adsorptive capacities of produced composites were evaluated in four oil samples. Functionalization of rGO was found to cause removal of residual oxygen containing functional groups such as hydroxyl (–OH), and resulted in more hydrophobic surface. Infusion of FrGO, in waste expanded polystyrene resulted into composites with increased surface area, from 71.50 m^2/g for pure PS_{20} to 353.45 m^2/g, 429.18 m^2/g, 456.14 m^2/g for PS_{20} infused with 1, 2 and 4wt% of FrGO. Increase in oil sorption capacities of the composite, observed in four oil samples corresponds to improved surface area. Produced composites show good recyclability in the four oil samples, at least up to the third sorption cycle.

✉ Samuel Ayodele Iwarere, samuel.iwarere@up.ac.za; ✉ Baba El-Yakubu Jibril, byjibril@gmail.com | [1]Department of Chemical Engineering, Faculty of Engineering, Ahmadu Bello University, Zaria, Kaduna State, Nigeria. [2]National Oil Spill Detection and Response Agency (NOSDRA), Ilorin Zonal Office, Federal Secretariat, Fate Road, Ilorin, Nigeria. [3]Department of Chemical Engineering, Faculty of Engineering, Built Environment and Information Technology, University of Pretoria, Hatfield, South Africa. [4]Department of Water Resources and Environmental Engineering, Ahmadu Bello University, Zaria, Kaduna State, Nigeria.

Graphical Abstract

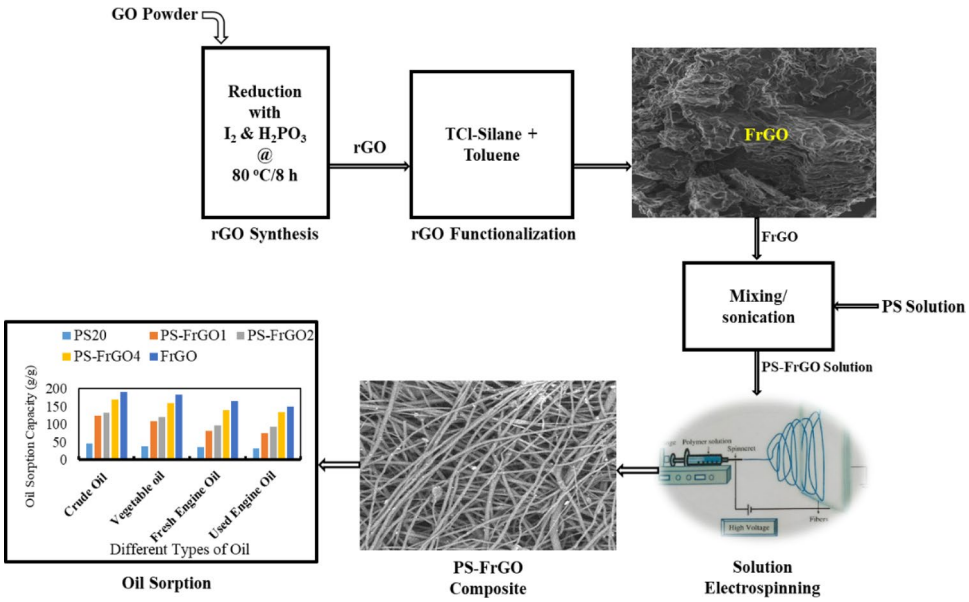

Highlights

- Modification of Graphene oxide (GO) to reduced Graphene Oxide (rGO)
- rGO was functionalized and infused in Polystyrene (PS) to form PS/FrGO composite
- PS/FrGO composite was applied to oil–water mixture for oil adsorption
- Reusability of composites produced was evaluated.

Keywords Graphene · Functionalization · Composite · Adsorption · Reusability

1 Introduction

Oil Spill is a global phenomenon and over the years, its clean-up has become a major challenge. Oil Spill incidences such as Mauritus Spill of 2020 (4000 barrels), Bonga Spill of 2011 (40,000 barrels) and Gulf of Mexico Spill of 2010 (4 million barrels) among numerous other oil spills, caught the world`s attention. Between January, 2021 and December 2022, there were over 1,025 reported cases of oil spill incidences in Nigeria, 612 of which was crude oil spills, 67 was condensate and 73 was refined products spills [1]. Sources of oil spills include leakages of pipelines, drilling activities, failures of equipment, natural disasters, accidental release during tank cleaning activities and third-party interference. Oil spills have been reported to have caused a lot of ecological problems [2].

Methods of cleaning oil contaminated waters have been classified into physical, chemical and biological. Examples of physical methods include booms and skimmers, flotation methods (column flotation, dissolved air, electro and induced air flotation), electro-coagulation and coalescence [3], gravity separation, membrane filtration, vacuum techniques, use of oil sorbents and reverse osmosis. Chemical methods such as in-situ burning, application of solidifiers, use of dispersants, breakers and emulsion inhibitors [4, 5], as well as chemical coagulation. Biological methods include bioremediation, use of biological agents for decomposition of petroleum hydrocarbons and membrane bioreactors.

These methods have been reported to be efficient for oil removal from water, however some of them suffers a few drawbacks. For instance, In-situ burning leads to secondary pollution, effects of wind on combustion process makes it unsuitable for petroleum pollutants cleanup in all geographical locations, controlled burning requires modern and

expensive equipment [6–9]. Chemical dispersants involves addition of chemicals to the sea and thereby causes potential toxicity. Ultra and micro filtration could be expensive for handling large spills. Mechanical treatment (booms and skimmers) are energy, equipment and labour intensive and ineffective for oil on turbulent waters [10–12]. Bioremediation are known to be a slow process which requires long time and are associated with air pollution and generation of residual viscous oil.

Due to its simplicity, low capital and operational cost, high removal efficiency, as well as environmental friendliness, adsorption has been known to be an optimal process, among other oil spill cleanup methods. However, during oil spill cleanup, caution must be exercised in using oil sorbents and other consumables, so as to minimize waste generation. It has been reported that volume of waste generated after oil spill clean-up could be, as much as ten times volume of oil originally spilt, [13]. Sorbents used in oil spill cleanup has been classified into three; natural organic, natural inorganic and synthetic organic sorbents. Natural organic sorbents such as corn stalk, bagasse pith, cotton fibers and nonwoven wool [14], are known to have low sorption capacities, as well as high-water absorption tendencies leading to loss of buoyancy. Natural inorganic sorbents such as zeolites, exfoliated graphite, vermiculite [15], are sensitive to fouling. Synthetic organic sorbents such as polyurethane, polypropylene, polyethylene and butyl rubber are non-biodegradable.

Limitations of these classes of sorbents, and the drive to meet industrial expectations necessitate fabrication and application of sorbents with higher sorption capacities and their availability at relatively low cost. Such sorbents include carbon-based nanoparticles such as reduced Graphene Oxide (rGOs), Carbon nanotubes (CNTs), Carbon nanofiber (CNF) among many others. These materials possess desirable adsorption properties such as high porosity, pore volume, well-developed structures, large specific surface area as well as, high oleophilic and hydrophobic nature, which are responsible for their superior performance [16]. The use of these nanoparticles as fillers in polymeric adsorbents, to improve adsorption properties of produced composites, had been fully established [17]. Wettability of most electrospun membranes are mainly affected by surface roughness and available functional groups [18]. Therefore, to obtain composites with super-wetting properties with high efficiency and selectivity in separating water and oil, modifying functional groups and surface roughness is of essence.

RGO surface essentially contain, hydrophilic functional groups such as the carboxyl (-COOH), carbonyl (C=O) and hydroxyl (-OH) groups. Extremely high surface area and porosity, outstanding mechanical, chemical stabilities and ease of chemical modification of rGO surfaces is currently been exploited to produce membranes with promising efficiencies [19]. When surface properties of rGO are modified, its chemical affinities, selectivity and sorption capacity for targeted molecules improved significantly. Surface modification of rGO is capable of enhancing its physical features such as porosity (> 87%), bulk density (14.4 mg cm^3), hydrophobicity (contact angle of about 144°) and mechanical stability [20]. However, there is scanty information in literature on the functionalization effects of rGO on sorption properties of its composites with polystyrene as oil sorbents.

Consequently, to fully understand the effects of surface modification of rGO on sorption properties of composites produced, with the surface modified rGO infused in waste PS, more work is needed. Therefore, the main contribution of this study is to investigate the effects of surface modification of rGO on the surface area, wettability and oil adsorption capacity of the composites produced when surface modified rGO is infused into waste polystyrene solution.

2 Experimental details

2.1 Materials

Natural Graphite (50μ), Iodine resublimed (I_2, 99.5%, Aldrich), N, N-Dimethylformamide (Analar), Hypophosphorous Acid, H_3PO_2 (50wt% in H_2O) and Trichloro (1H, 1H, 2H, 2H-heptadecafluorodecyl) silane (96%, Tcl) were supplied by Sigma-Aldrich. Sodium Nitrate, $NaNO_3$ (99%), Hydrogen Peroxide, H_2O_2 (30%), Potassium permanganate, $KMnO_4$ (99%), Sulphuric Acid, H_2SO_4 (98%) and Hydrochloric acid, HCl (37%) were purchased from Glassworld Chemical Suppliers, South Africa. Polystyrene waste plastic was collected from an electronic store at Oyo, Nigeria. Fresh engine oil and vegetable oils were purchased from a gas station and shopping mall respectively, in Ogbomosho, Nigeria. Used engine oil was collected from an automobile workshop at Under G along LAUTECH, Ogbomosho, Nigeria. All chemicals were used in its pure form as received from suppliers, and deionized water was used.

2.2 Preparation of reduced graphene oxide

Prior to this step, our group had earlier synthesized Graphene Oxide (GO) by modified Hummer's methods. 90 g GO powder was dissolved in 22.5 mL deionized water (4 mg/mL). Hypophosphorous Acid (H_3PO_2) acid (7.5 mL) was accurately measured and then mixed with the aqueous GO solution. 900 mg of iodine (I_2, 99.5%, Aldrich) was added to the suspension, to form a mixing ratio of GO: H_3PO_2: I_2 = 1:100:10. Sonication of the suspension was done in an ultrasonic cleaner (Model PS-80) for 5 min at a temperature of 30 °C, and was subsequently transferred into an oven (LABEX: FMH instruments; SHK-IN) where it was heated for 8 h at 80 °C. A black gel was formed after the heating. rGO wet gel was taken out of the oven, allowed to cool to room temperature in a fume cupboard. The rGO was then washed with ethanol and deionized water in a volume ratio 1:1, until a pH of neutral was attained. Finally, the as synthesized rGO was freeze-dried for 72 h.

2.3 rGO functionalization

100 mg of as synthesized rGO was weighed into a clean Petri-dish. 0.1 cm^3 of Trichloro (1H, 1H, 2H, 2H-heptadecafluorodecyl) silane (96%, Tcl) was subsequently dissolved in 30 mL toluene (99.8%, Sigma-Aldrich) and allowed to stand for about 1 h. rGO was soaked in the solution for 12 h in the Petri-dish, at room temperature, which was securely covered to avoid air interference. After 12 h, the solvent was decanted off, and the functionalized reduced Graphene Oxide was rinsed with deionized water. Functionalized rGO (FrGO) was finally dried overnight for 24 h in a vacuum oven at 40 °C.

2.4 Fabrication of PS-FrGO composites by electrospinning

Twenty weight percent of PS in DMF has been earlier established, to produce stable electrospun fibers during electrospinning [21, 22, 28]. In a 250 mL beaker, 20wt% PS was charged into N, N-Dimethylformamide and stirred vigorously on a magnetic stirrer (DATHAN MNH-20D) at 250 rpm for about 1 h, until it dissolved. Three different concentrations (1, 2 and 4wt%) of FrGOs were subsequently mixed with the 20wt% PS solution and then tagged PS-$FrGO_1$, PS-$FrGO_2$ and PS-$FrGO_4$ composite sorbents respectively. The composites were further stirred on the magnetic stirrer at 250 rpm for another 1 h, until homogeneity was obtained. The mixtures were then sonicated at 30 °C using an ultrasonic cleaner (Celsius Scientific-Model PS-80) for a duration of 30 min. To fabricate PS and PS-FrGOs composite sorbents, an IME Technologies Electrospinning Platform (V4 HMI engine MKI), which consist a DC high-voltage supply, a syringe pump, and rotating drum collector, was used. 10 mL of PS-FrGOs composite solutions were separately pumped into a 15 mL syringe, and then clamped. The syringe pump was subsequently set at 0.5 mL/hr. Rotating drum collector was lined with aluminum foil, set at 100 rpm and the D. C. voltage was set at 15 kV. Diameter of the needle used was 0.8 mm and a needle collector distance of 15 cm was observed. Electrospinning was performed at 28 °C and 64% relative humidity. Electrospun composite fibers were finally removed from the collector and placed in an oven which had been calibrated and previously set at 60 °C overnight, to evaporate residual solvent.

2.5 Characterization of FrGO and PS-FrGOs composite

Graphite (G), GO, rGO, PS and PS-FrGOs microstructures were obtained using a field emission scanning electron microscope, FE-SEM, (Zeiss Ultra Plus 55) which has EDX apparatus, operated at 2.0 kV. To obtain diameters of composites electrospun fibers, SEM images of the composite, was imported into Image J software. Fourier transform-infrared (FTIR) spectra of G, GO, rGO, FrGO, PS and PS-FrGOs were obtained with Varian FT-IR spectroscopy with wavenumber, in the range 500–4000 cm^{-1}. High resolution transmission electron microscope, HRTEM FEI Tecnai-F30, (JEOL-2100F) alongside 200 kV acceleration voltage, operated at 1.0 kV was used to obtain the transmission electron microscope (TEM) images of G, GO, rGO and FrGO. Bruker BV 2D PHASER Best Benchtop X-ray diffraction (XRD) analyzer with reflection geometry at 2θ values (5°–90°) and a step size of 0.005°, operated with a Cu $K\alpha_1$ radiation source (λ = 0.15406 nm) at 50 kV and 30 mA was used to analyze the Phase structure of (G), GO, rGO, PS and PS-FrGO. As-prepared G, GO, rGO and FrGO samples were characterized with WITec alpha 300 RAS + Confocal micro-Raman microscope operated at 532 nm laser

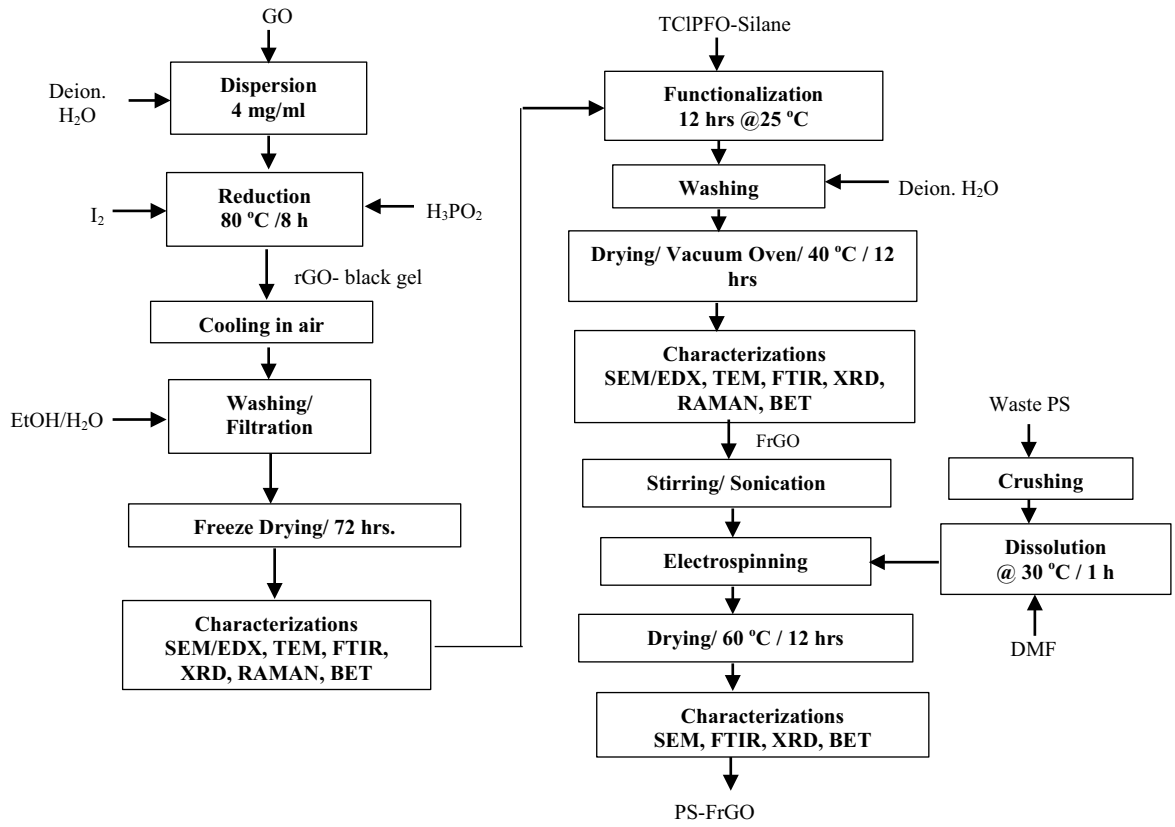

Fig. 1 Fabrication of PS-FrGO composite sorbent by solution blending and electrospinning method

wavelength with an acquisition time of 150 s and laser power of 5 mW on the sample so as to avoid heating the samples. G, GO, rGO and FrGO surface areas were determined by N_2 adsorption at 77.35 K (BET) using a St 1 on NOVA touch 2LX [s/n:1050003126] instrument, after degassing for 3 h at 373 K. Quantachrome instruments was used to determine the Surface areas of PS-FrGOs by N_2 adsorption at 273 K (BET), after degassing for 1 h at 373 K. The block diagram presented in Fig. 1 summarized all stages.

2.6 Oil sorption studies

2.6.1 Maximum oil sorption capacity

Oil sorption capacity of PS and composite PS-FrGO sorbents, at maximum was estimated in four oily-water samples, under a batch adsorption model. In the adsorption experiment, dry known weights of sorbents were left in oils for 60 min, until the sorbents get saturated, they were then taken out with a tweezer. Wet sorbent was allowed to drain for about 10 s, and then weighed dried. Subsequently, sorption capacity of produced sorbents was estimated with Eq. 1 as follows.

$$Q = \frac{M_a - M_b}{M_b} \tag{1}$$

where; Q = Maximum sorption capacity of sorbents (g/g); M_b = sorbent mass before oil sorption (g) and M_a = sorbent mass after oil sorption (g). Sorption experiments were conducted in triplicate at room temperature, so that the results could be repeatable.

2.6.2 Oil sorption kinetics

Kinetics of oil sorption established the relationship between adsorbate concentration in solution and rates of oil uptake. It further assists in deriving important information on the mechanism controlling the adsorption process, time needed to attain equilibrium, as well as adsorbent-adsorbate interaction pathways. Three kinetics models were utilized to study the kinetics of four oil samples on the produced composites, PS-FrGOs. These models include pseudo-first-order (PFO), pseudo-second-order (PSO) and intraparticle diffusion (IPD) models.

Equation (2) and (3) described the Pseudo first-order kinetic model, [32]

$$\frac{dq_t}{dt} = k_1(q_1 - q_t) \tag{2}$$

$$ln(q_e - q_t) = lnq_e - k_1 t \tag{3}$$

where; q_t is adsorbate amount adsorbed at any time t, g/g; q_e is amount of adsorbate adsorbed at equilibrium, g/g; and k_1 is pseudo-first order rate constant, in min^{-1}.

Equation (4) and (5) described pseudo second-order model, based on the equilibrium adsorption capacity [23, 32]

$$\frac{dq_t}{dt} = k_2(q_e - q_t)^2 \tag{4}$$

$$\frac{t}{q_t} = \frac{1}{K_2 q_e^2} + \frac{t}{q_e} \tag{5}$$

where; q_t is adsorbate amount adsorbed at any time t, g/g; q_e is amount of adsorbate adsorbed at equilibrium, g/g; and k_2 is pseudo-second order rate constant, in g/g min.

To describe the oil sorption mechanism, the intraparticle diffusion model was utilized. As shown in Eq. (6), one adsorption can be divided into multiple linear equations, [23, 32]

$$q_t = k_{dif} t^{1/2} + C \tag{6}$$

where; q_t is amount of oil adsorbed at time t, g/g; and k_{dif} is the intraparticle diffusion rate constant, in $g/gmin^{0.5}$. C is a constant, which is the intercept of the straight line graph, and related to the thickness of the boundary layer (g/g).

Based on the experimental data obtained from sorption of oil, straight equations were fitted and regression coefficients, the (R^2) value were calculated so as to investigate fitness the models.

2.7 Desorption test and sorbents reusability

Oil-ladened composite sorbents was compressed between two flat plates to desorb the oil sorbed by PS and PS-FrGO composites. They were rinsed later in ethanol solution and then in deionized water. They were finally dried at 60 °C in an oven for about 15 min, and the sorption–desorption cycles continued until the composites collapse physically.

3 Results and discussion

3.1 Morphological structures of G, GO, rGO, FrGO

In the morphology of graphite (G), there is no definite pore structure. In rGO, flexible sheets of graphene overlapped and coalesce, thereby formed well-defined 3D framework which is porous in nature. Similar morphologies for rGO have been reported by, Wang et al. [24] as well as Pin-Hsuan et al. [25]. Upon modification of the rGO surface, stacking of graphene sheets was not affected. Figure 2a, shows morphology of these samples. Similarly, in the TEM images

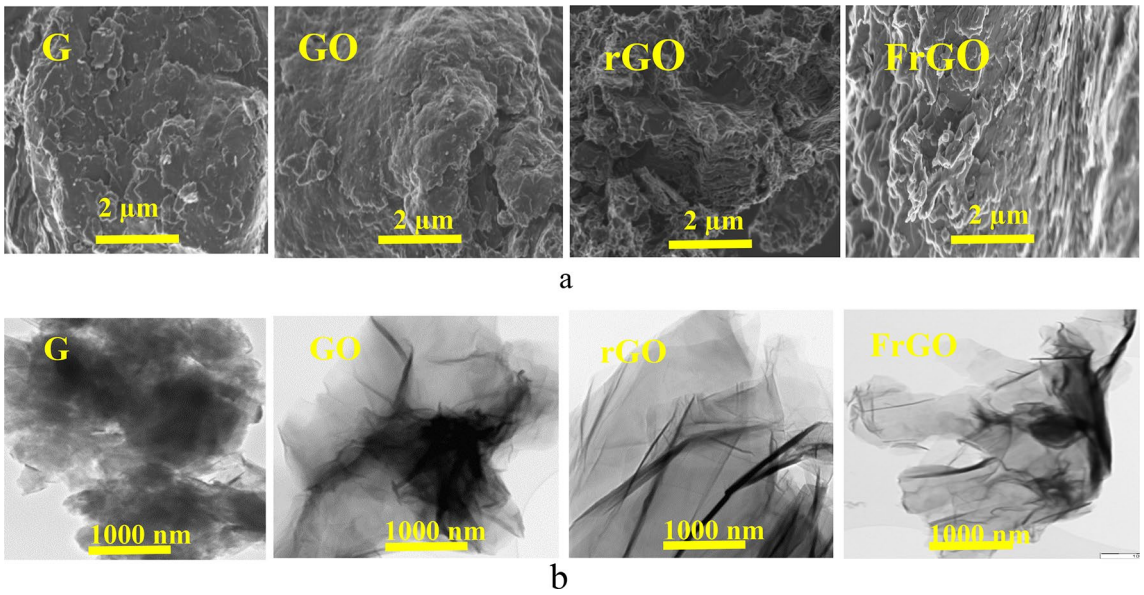

Fig. 2. **a** Morphologies of Graphite, Graphene Oxide, reduced Graphene Oxide and functionalized rGO; **b** TEM images of Graphite, Graphene Oxide, reduced Graphene Oxide and functionalized rGO

shown in Fig. 2b, graphite (G) shows a tight aggregate within host sheets, with the formation of bulk nanostructure, and no distinctive sheet as well as exhibition of lower interlayer spacing. Thinner flaky, wrinkles and folds were formed from dispersed aggregated sheets in GO. A 3D network which depicts strong interconnection between building blocks of the GO, was shown. This finding is consistent with the report of Pin-Hsuan et al. [25]. In rGO, at the edges of graphene sheets as compared to GO, more wrinkles, twists and folds are observed. rGO was seen to exhibits cellular structure inside, with pores that are interconnected. Assembled graphene sheets, are the building blocks of these pore walls. This implies that graphene sheets cross-linked to produce 3D porous structure and later assembled to form larger sheets, similar results was reported by Pin-Hsuan et al. [25]. TEM image of FrGO shows few layers of graphene sheets which stacked on each other.

3.2 EDX of G, GO, rGO and FrGO

EDX spectrum of natural graphite (G) shows that it is primarily composed of carbon with a trace of silicon. GO is composed of 76.75% carbon, 22.72 oxygen, 0.04% potassium and 0.48% Sulphur. rGO is essentially carbon and oxygen with traces of phosphorous and silicon. There was a significant decrease in its oxygen composition from about 22.72% to 12.50% after the reduction of GO to rGO with Hypophosphorous Acid and Iodine. After functionalization to FrGO, additional element such as Fluorine was found on its surface, with a further reduction of oxygen content to about 10.19%, which suggests further removal of oxygen containing functional group from rGO surface. 4.67% Fluorine on FrGO indicates successful introduction of Fluorine to the surface of rGO after functionalization showing an agreement with the reports of Ren et al. [26]. Figure 3 shows the EDX spectra of produced samples.

3.3 FTIR spectra of G, GO, rGO and FrGO

For G, at 3638 cm^{-1}, 2191 cm^{-1} and 1727 cm^{-1} represent nonbonded hydroxyl (-OH) group stretch, triple bonds (C≡C) stretch and vibrations of unsaturated (C=C) double bond, which are all faint peaks. This observation aligned with the results of, Faniyi et al. [27]. Spectrum of GO shows, typical peaks at 3185 cm^{-1}, 1715 cm^{-1}, 1618 cm^{-1}, 1224 cm^{-1}, 1049 cm^{-1} and 971 cm^{-1} which are respectively assigned to O–H stretch, Carbonyl (C=O) stretching, aromatic ring (C=C–C) ring, epoxy (C-O) stretching, alkoxy (C-O) stretching and trans (C-H) hydrogen group. Upon reduction of GO to rGO, the peaks at 1385 cm^{-1} and 1715 cm^{-1} are absent, and the peak at 1224 cm^{-1} was found to be broadened and weakened in intensity. This simply implies oxygen containing functional groups were removed during reduction process, which totally

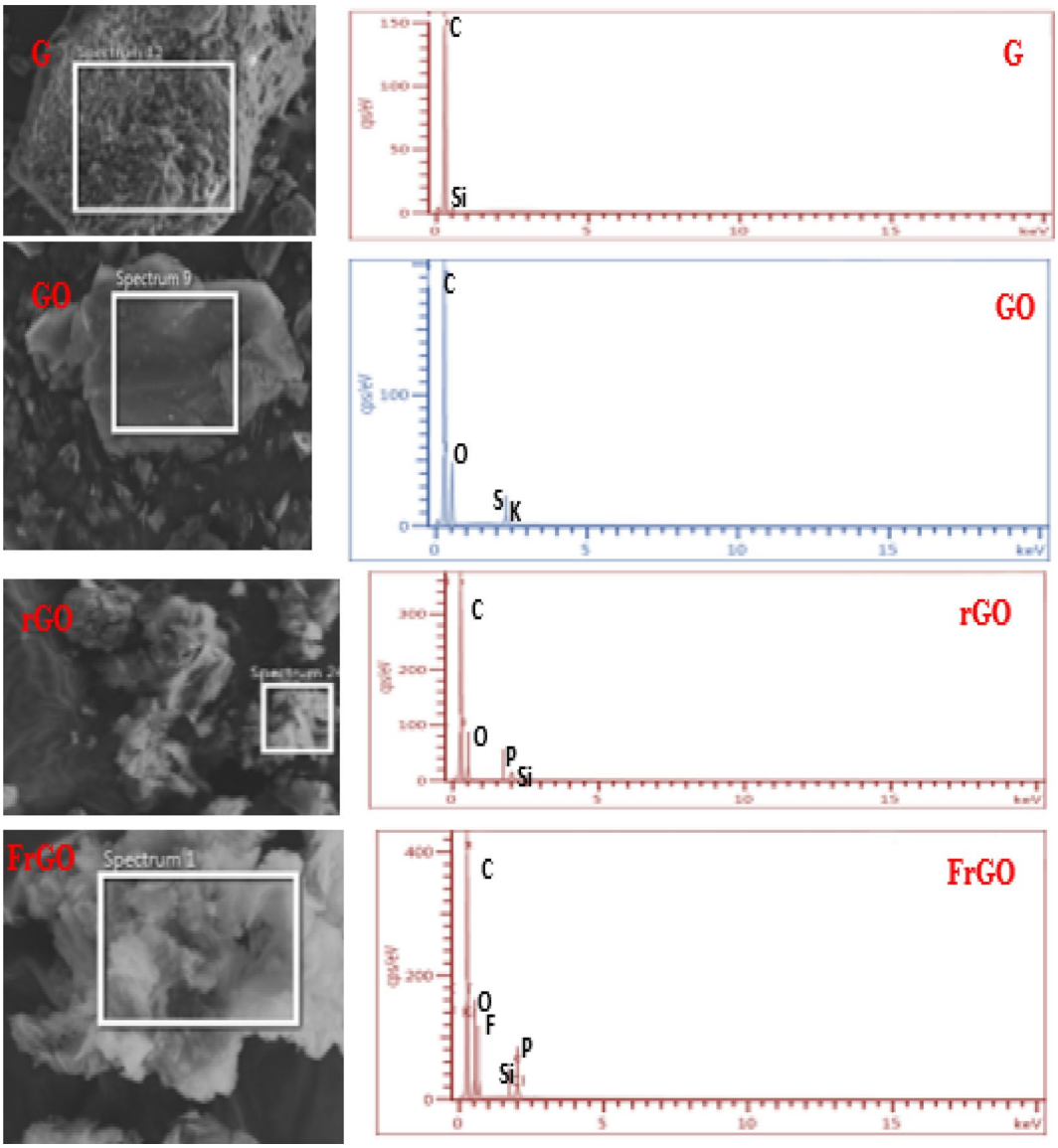

Fig. 3 EDX Spectra of natural graphite, reduced graphene oxide and functionalized reduced graphene oxide

agrees with the report of, Oribayo et al. [28]. For Surface modified rGO, peaks at 1606 cm^{-1} and 1139 cm^{-1} correspond to aromatic ring (C=C–C) ring and aliphatic fluoro (C-F) compound respectively, which are faint. A sharp peak was also shown at 1267 cm^{-1} assigned to primary hydroxyl (- OH) in-plane bond, which is similar to the report of Jin-Yong et al. [20]. G, GO, and rGO spectra and its surface modified form are presented in Fig. 4a.

3.4 XRD patterns of G, GO, rGO and FrGO

XRD according to the matching card number JCPDS N96-120–0018 was adopted in analyzing phase-structure of synthesized samples. In G, the narrow diffraction peak at $2\theta = 26.02^0$ corresponds to interlayer spacing of 3.35 Å, and after oxidation of G to GO, this peak disappeared to form a new peak at $2\theta = 11.07^0$ corresponding to an interlayer spacing of 7.97 Å. This implies that interlayer spacing of carbon structure increases along with oxidation, Wang et al. [24] had earlier reported a similar view. Upon reduction of GO, a new, faint and much broadened peak appeared at $2\theta = 23.14^0$ which

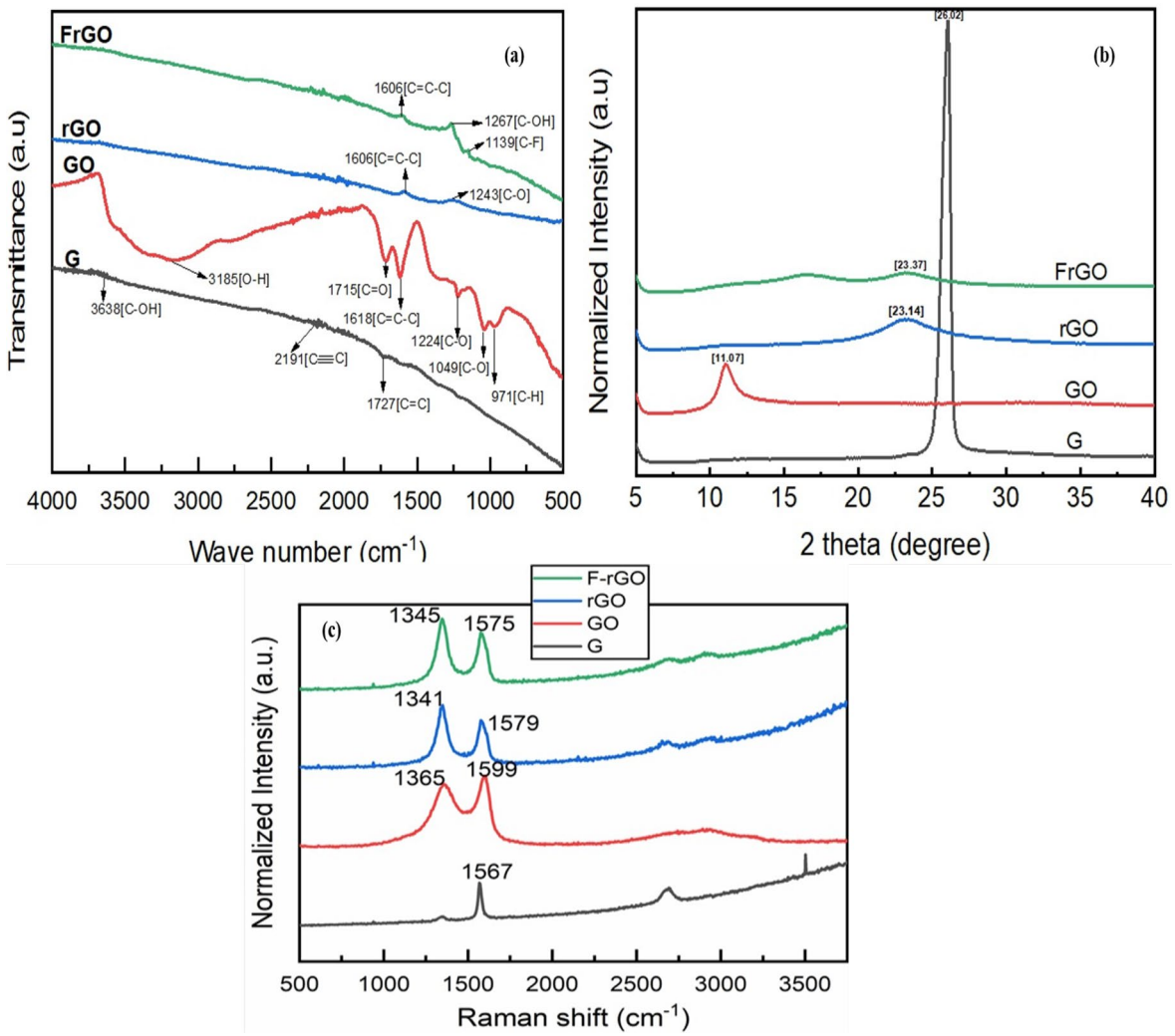

Fig. 4. **a** FTIR spectral of Graphite, Graphene Oxide, rGO and FrGO **b** XRD patterns of Graphite, Graphene Oxide, rGO and FrGO, **c**—Raman Spectra of Graphite, Graphene Oxide, rGO and FrGO

corresponds to interlayer spacing of 3.82 Å, and depicts the pattern of amorphous carbon structure in as synthesized rGO. rGO was seen to migrate to a lower 2θ angles compared to G, this indicates that, there is a change of interlayer spacing, suggesting that the interlayer spacing of rGO layers is larger in rGO than in G. These suggest that reduction of GO to rGO successfully occurred during chemical reduction step, and consistent with the reports of Pin-Hsuan et al. [25]. After functionalization of rGO the peak at 23.14 shifted slightly to 23.37 which correspond to a d spacing of 3.81 Å. This further implies that amorphous nature of the rGO is almost unaffected by its functionalization. The XRD patterns of G, GO, rGO and FrGO measured within angular range $2\theta = 5^0$–40^0 were presented in Fig. 4b.

3.5 Raman spectra of G, GO, rGO and FrGO

Molecular structures of G, GO, rGO and FrGO samples was studied with Raman spectroscopy measurement. For graphite (G), a sharp G-band at 1567 cm^{-1} and a faint D-band at 1353 cm^{-1} corresponds to disordered graphitic lattice. Ratio of intensities of D peak to G peak (I_D/I_G), is used to establish the density of defects in carbon materials. That of graphite is 0.20 which implies that it is in its undisturbed graphitic form. Upon oxidation of graphite, the G-band and D-band of GO appeared at 1599 cm^{-1} and 1365 cm^{-1} respectively which depicts a disordered graphitic lattice, with I_D/I_G being 0.94. For rGO and FrGO, existence of D-band at 1341 cm^{-1} and 1345 cm^{-1} and those of G-band at 1579 cm^{-1} and 1575 cm^{-1}

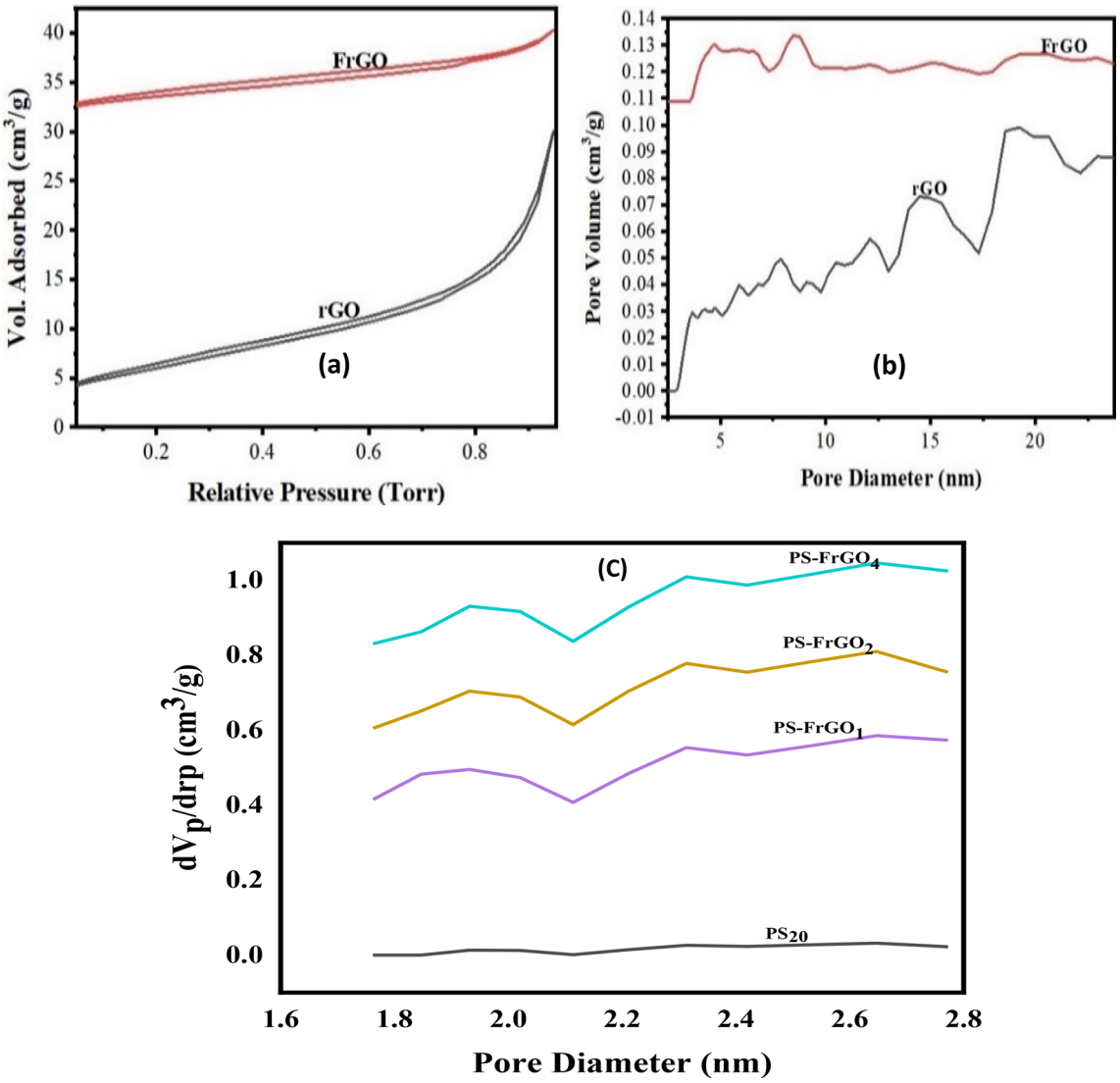

Fig. 5. **a** Nitrogen adsorption–desorption isotherms of rGO and FrGO. **b** DFT pore distribution curves of rGO and FrGO. **c** Pore size distribution of PS_{20} and PS-FrGO Composites

respectively, near standard locations of graphene at 1350 cm^{-1} and 1580 cm^{-1} confirms the presence of graphene in rGO and in its surface modified form. Ratios of peak intensities of D-band to G-band of rGO and FrGO are 1.06 and 1.05 respectively, which further implies that as synthesized rGO is highly defective, and surface modification does not cause further defect in the FrGO structure, this result agrees with the reports of Hoai et al. [29]. Raman spectra of the four samples are presented in Fig. 4c.

Table 1 Pore sizes, pore volumes and BET surface areas of G, GO, rGO and FrGO

Materials	Average Pore Size (nm)	Total Pore Volume (cm^3/g)	BET Surface Area (m^2/g)
G	8.2519	0.0133	16.608
GO	7.6245	0.0316	81.083
rGO	6.3651	0.0465	140.570
FrGO	3.6002	0.0729	156.360

Table 2 DR-Plot Pore diameters, DR-Plot Pore volumes and Surface Areas of composites

S/No	Composites	Pore diameter (nm)	Pore volume (cm^3/g)	BET surface area (m^2/g)
1	PS20	6.435	0.0252	71.50
2	PS-$FrGO_1$	5.842	0.1522	353.453
3	PS-$FrGO_2$	6.181	0.1652	429.183
4	PS-$FrGO_4$	6.243	0.1746	456.143

Table 3 Fiber diameter of electrospun composites sorbents from their SEM images

S/NO	Composites	Average Fiber Diameters (μm)
1	PS_{20}	2.855
2	PS-$FrGO_1$	5.722
3	PS-$FrGO_2$	5.508
4	PS-$FrGO_4$	2.620

3.6 Specific surface area

3.6.1 Specific surface area of rGO and FrGO by BET

In both rGO and its surface modified form, FrGO, a Type IV adsorption–desorption isotherm with Type H3 hysteresis loop are observed, this corresponds to the existence of mesopores. This is presented in Fig. 5a. Similarly, from the pore size distribution of rGO and FrGO based on density functional theory (DFT) and displayed in Fig. 5b, the pore diameters of rGO and FrGO are 6.36251 nm and 3.6002 nm respectively, which show that both rGO and FrGO are in mesoporous porosity range. After surface modification of rGO to FrGO, a significant decrease in pore diameters is observed, there was no significant mesopore blocking after chemical modification by silane. This agrees with the report of Jin-Yong et al. [20]. Their pore volumes are 0.04656 cm^3/g and 0.07298 cm^3/g, and BET surface area are 140.5709 m^2/g and 156.3606 m^2/g respectively. Obviously, functionalization of rGO caused a slight increase in the BET surface area of FrGO. Figure 5a and b, present adsorption–desorption isotherm and pore distribution based on density functional theory (DFT) for both rGO and FrGO respectively. A summary of the average pore size, pore volume and BET Surface area of the four samples is presented in Table 1.

3.6.2 BET surface area of PS_{20} and PS-FrGOs composite sorbents

Pore distribution of PS_{20} and PS-FrGO composites based on Density Functional Theory (DFT) are presented in this section. Figure 5c, and Table 2 shows their pore diameters and pore volume, obtained by DR-plot (micropore volume) method, as well as, BET Surface Area of composites. As evident from Fig. 5b, pore diameters of both PS_{20} and its composites are all higher than 2 nm which implies that they all exist in the mesoporous regions. It is observed from Table 2 that pore volume slightly increases as the ratio of FrGO in PS_{20} increases. Similarly, the surface area of PS-$FrGO_1$ is about five times that of PS_{20}, while those of PS-$FrGO_2$ and PS-$FrGO_4$ are six times that of PS_{20}. These results confirm that infusion of FrGO, with high pore volumes and surface area, in waste polystyrene solution results in a proportionate increase in the surface area of composites. These results agree with the report of Lin et al. [30]. Functionalization of rGO causes further removal of residual oxygen containing functional groups such as hydroxyl (-OH) group and eventually resulted in a highly hydrophobic composite surface with very high surface area.

3.7 Morphology of electrospun PS and PS-FrGOs composite sorbents

Morphology of the produced composites shows fibers with random orientation in a self-sustained web. This result agrees with the reports of Al-Azab et al. [31]. Morphology of each sample was further assessed by quantitative analysis with about 100 counts of fiber diameters taken from SEM images using Image J software, and average fiber diameter of each

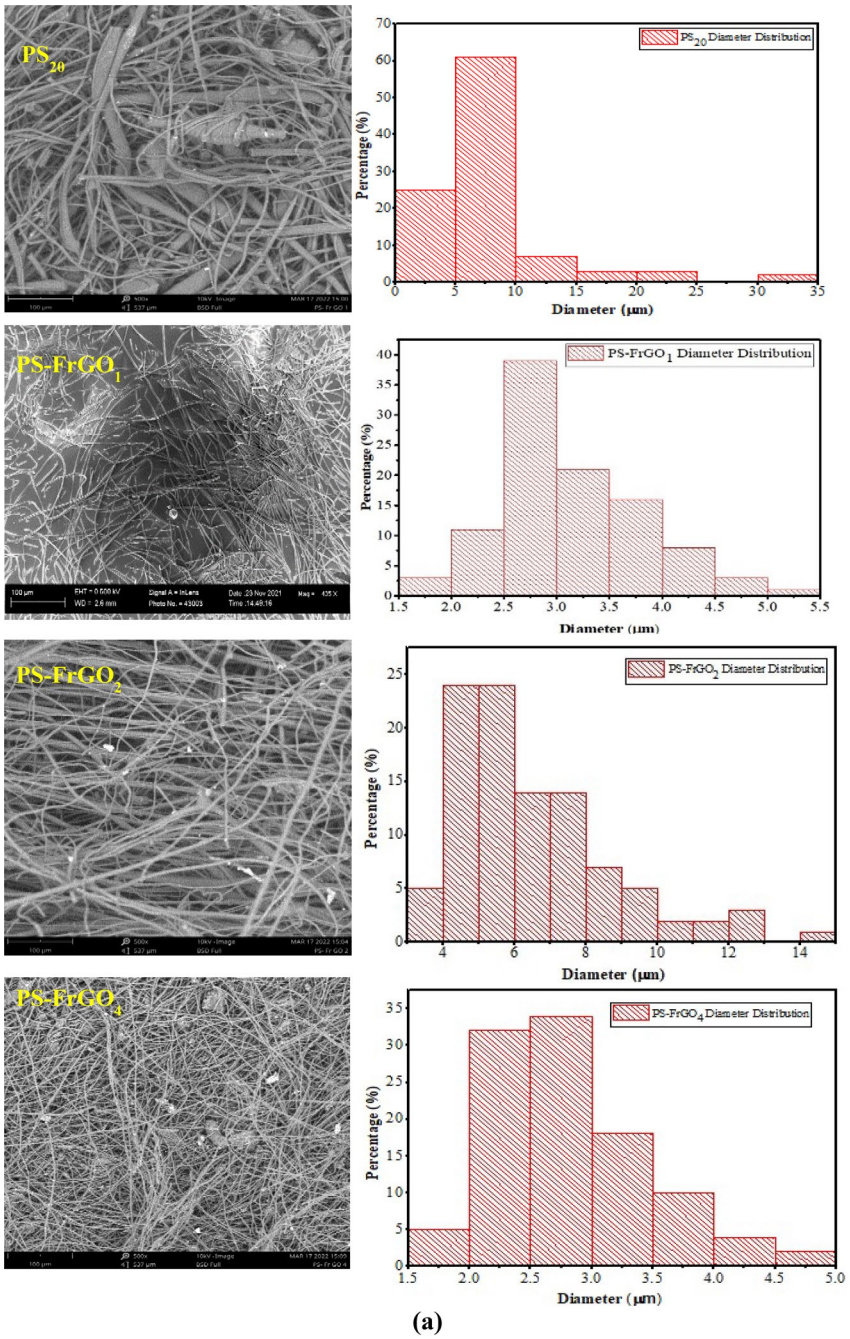

Fig. 6. **a** Morphology of electrospun PS infused with FrGO and Fiber Diameter Distribution, **b**—SEM Images PS_{20} and Interaction of PS with FrGO at different Concentration

composite is presented in Table 3. Electrical conductivity of PS-solution and dispersion of FrGO in the polymer solution determines the morphology and fiber diameter of electrospun sorbents. As evident from Table 3, PS-FrGO$_4$ has slightly lower fiber diameter compared to PS$_{20}$ because infusion of FrGO increased the electrical conductivity of PS-Solution, its elasticity and tendency to stretch towards the collector, thereby producing narrower diameter fibers. However, PS-FrGO$_1$ and PS-FrGO$_2$ are observed to produce fibers with higher average diameters possibly due to uneven dispersion of FrGO in the PS-solution. Figure 6a shows the SEM images of PS and PS-FrGO composites as well as their fiber diameter distribution plotted on histograms to determine the distributions of fiber diameter. Figure 6b shows the interaction of FrGO particles attached to the surface of the PS after electrospinning.

3.8 XRD patterns of FrGO, electrospun PS$_{20}$ and PS-FrGOs sorbents

In the XRD patterns of FrGO, PS$_{20}$ and PS-FrGO$_1$, PS-FrGO$_2$ and PS-FrGO$_4$, FrGO shows diffraction peaks at 16.72 and 23.14 and 42.97 and as earlier mentioned, functionalization does not affect the amorphous nature of rGO. PS$_{20}$ shows diffraction peaks at 19.11°, 29.16° and 34.34. Infusion of 1 and 2 weight % FrGO into the PS matrix caused no new diffraction peaks to form, which implies that, at these concentrations, the parallel and regular layered structure of FrGO got lost when dispersed in the polystyrene matrix. When 4 weight % of FrGO was infused into the PS, a new diffraction peak is

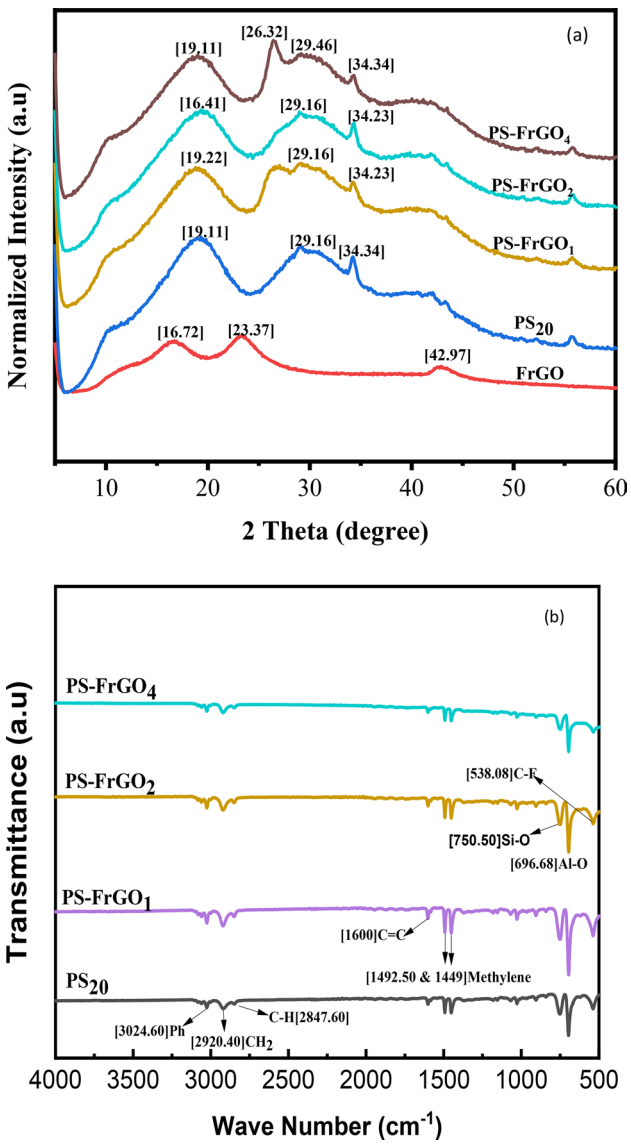

Fig. 7. **a** XRD patterns of FrGO, PS$_{20}$ and PS-FrGO$_1$, PS-FrGO$_2$ and PS-FrGO$_4$, **b**—FTIR Spectra of PS$_{20}$ and PS-FrGO composite sorbents

shown at 26.32°, which implies that, higher concentration of FrGO may not agglomerate in the PS_{20} matrix. XRD patterns of these samples are shown in Fig. 7a.

3.9 FTIR of PS_{20} and PS-FrGOs composite sorbents

FTIR Spectra of PS_{20} and PS-FrGO alike show three distinct peak regions, which are common to all composites. 3024.60 cm^{-1}, 2920.40 cm^{-1} and 2847.60 cm^{-1} correspond to the stretching vibration of phenyl group (Ph), CH_2 and C-H respectively. Peaks at 1600 cm^{-1}, 1492.50 cm^{-1} and 1449 cm^{-1} in the second region, are assigned to the vibrations of olefinic conjugated C = C bond as well as those of methylene respectively. In the third region, peak at 750.50 cm^{-1} correspond to Si–O stretch and that at 696.68 cm^{-1} correspond to stretching vibration of Al-O. It was observed that, location of peaks representing specific functional groups are nearly the same in PS_{20} and PS-FrGOs. This simply shows that infusion of FrGO into the polymer matrix does not affect the segmented structure of polystyrene, which implies that infusion of FrGO into PS_{20} only contribute to the hydrophobic nature of resultant composite. This therefore confirms that there is no chemical interaction between FrGO and PS_{20}, FrGO only acts as a nanofiller. This observation agrees with those reported by Lakayan et al. [32]. Figure 7b presents the FTIR Spectra of PS_{20} and PS-FrGO composite sorbents.

3.10 Performance evaluation of PS_{20} and PS-FrGO composite as oil sorbents

The composites produced in this study are mops for spilled oil on water, compared with polypropylene-chitosan sponges produced by Abeer et al. [33] as well as aminoalkylsilane-grafted cotton fabricated by Abeer et al. [34], which are both filter screen for separating oils from water. The two sets could be applied for oily water separation but along different lines of operation. The sorption mechanism of the sorbents produced in this study is that, both adsorption and absorption occurs simultaneously. Oil molecules diffused into the micro-sized space between interconnected nanofibers due to oleophilic properties of the sorbent. The molecules further migrate to the micro and nano-pores on the fibers surface by capillary forces, and filled into the voids between PS and FrGO. In the final step, the absorbed oil molecules were held in the pores by van der Waal forces.

In four oils samples tested, PS-$FrGO_4$ has the highest oil sorption capacity, these could be due to its modified surface properties, improved specific surface area, as well as thinner fiber diameters. Oil sorption capacity also increases as the concentration of FrGO in PS increases from 1wt% to 4wt%. This result was compared with those of Mookgo et al. [35] where the sorption capacity of crude oil and sunflower oil increases with loading of modified CNT on polyvinylidene fluoride (PVDF) polymer. Similarly, the result agrees with the account of Lakayan et al. [32] which reported that, the rate of motor oil, vacuum pump oil and gasoline sorption increases by increasing the concentration of Cloisite 20A in PS. As presented in Table 3, Fiber diameters of PS-$FrGO_1$ is slightly larger than PS-$FrGO_2$, and its oil sorption capacity lower than that of PS-$FrGO_2$, as compared to PS-$FrGO_4$, which possess a much smaller electrospun fiber diameter size. Pure PS has much lower sorption capacities compared to Pure FrGO and the PS/FrGO composites because it have significantly low specific surface area. From the oil sorption mechanism, additional pores on the PS fiber after infusion of FrGO implies increase in the pore volumes and the BET Surface area. This is further illustrated by the SEM images of the composite in Fig. 6b, and presented in Table 2. Adsorption being a surface phenomenon, implies that, as surface area and pore volumes of the composites increases due to infusion of FrGO on PS, oil sorption capacities also increases.

Maximum Oil sorption capacity of three composite sorbents based on PS and FrGO mixtures (PS-$FrGO_1$, PS-$FrGO_2$, PS-$FrGO_4$), those of purePS and FrGO, in four oil samples, are presented in Fig. 8. Sorption capacities of pure PS in the four oil samples is (32.57–46.32) g/g. Those of PS infused with 1wt% FrGO in the four oil samples ranges from (74.86–123.81) g/g. This result signifies that sorption capacities of PS improved significantly with infusion of FrGO. As compared with the sorption capacity of commercially available non-woven polypropylene sorbent reported by Oribayo et al. [28], which ranges within (7–15) times its own weight. PS-FrGOs composite sorbent produced in the current study, was found to have much higher sorption capacities than those of commercially available non-woven polypropylene.

Oil sorption capacity attained by PS-$FrGO_4$ in four oil samples is in the range (133.55 – 168.83) g/g. These values are larger than oil sorption capacity of polyvinylidene fluoride (PVDF) and carbonnanotubes (CNTs) composites in crude oil, reported by Abeer et al. [33]. Polystyrene/lignin /OV-POSS nanocomposite monolith produced by Abeer et al. [36] also showed separation efficiency above 90% which in the same range with those of the composites produced herein this research. Similarly, the composites produced in this research shows sorption capacity in the same range

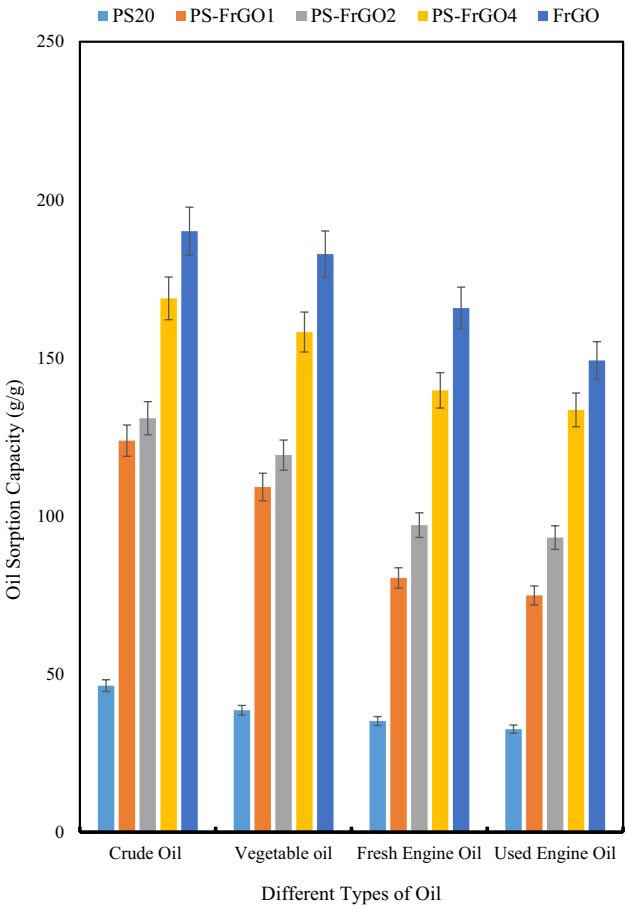

Fig. 8 Maximum oil sorption capacities of composite sorbents

Table 4 R^2 and SSE (%) values of different kinetic models for the four types of oil used

Oil Samples	Kinetic Models	R^2	SSE (%)
Crude Oil	PFO	0.9509–0.9887	0.4217–1.9185
	PSO	0.9849–0.9872	5.5930–9.2522
	IPD;		
	R_1^2	0.9332–0.9872	–
	R_2^2	0.9625–0.9956	–
Vegetable Oil	PFO	0.5922–0.9565	1.9852–9.8838
	PSO	0.9921–0.9993	0.4069–1.6062
	IPD;		
	R_1^2	0.9357–0.9771	–
	R_2^2	0.7038–0.9486	–
Fresh Engine Oil	PFO	0.808–0.9835	1.1442–7.0644
	PSO	0.9938–0.9992	0.4366–1.4977
	IPD;		
	R_1^2	0.9419–0.9699	–
	R_2^2	0.8405–0.9647	–
Used Engine Oil	PFO	0.8498–0.9667	0.3216–5.2163
	PSO	0.9871–0.9988	0.8207–2.0289
	IPD;		
	R_1^2	0.8905–0.9911	–
	R_2^2	0.6571–0.9911	–

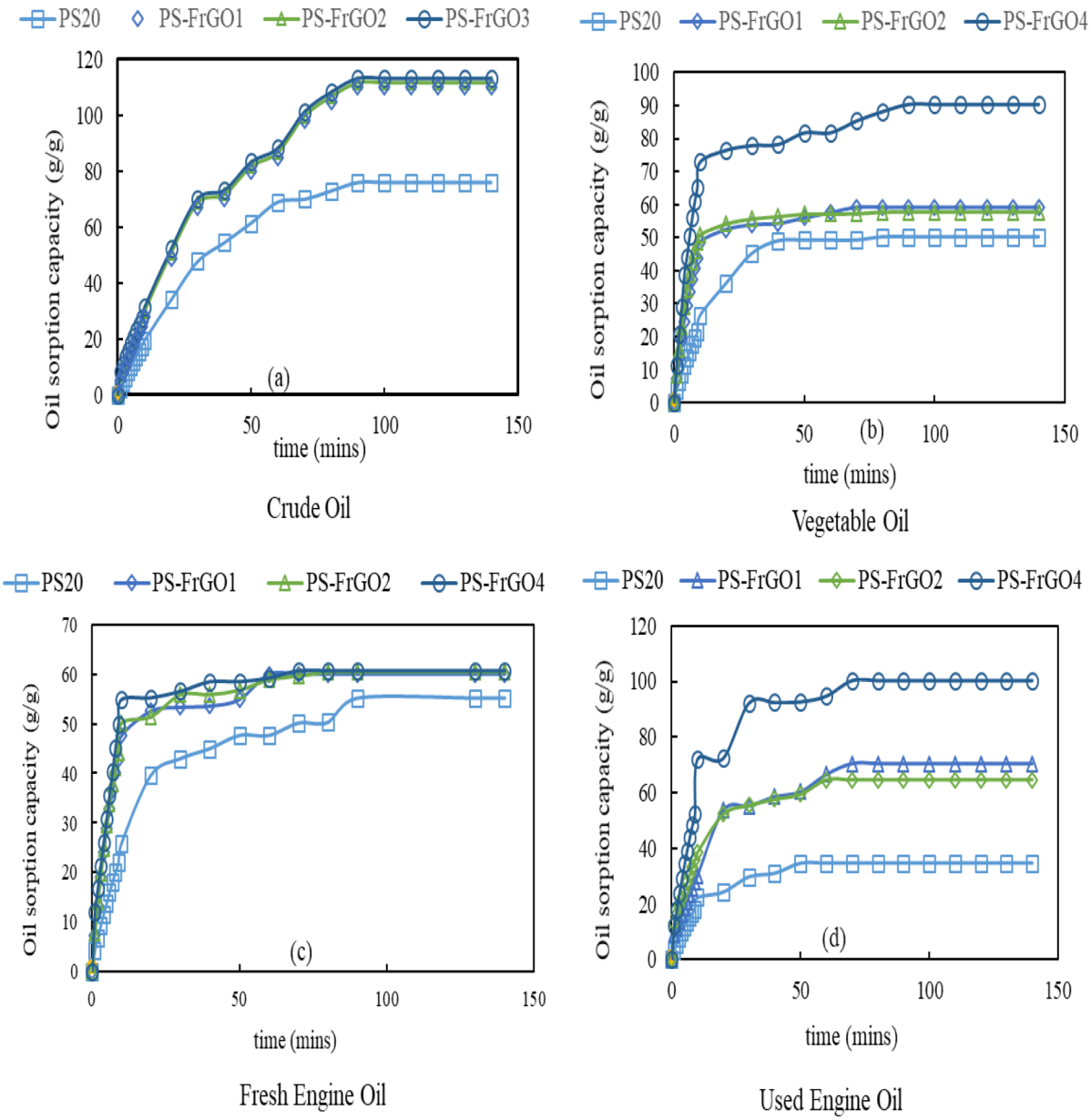

Fig. 9 Oil sorption kinetics of seven different sorbents (PS20, PS-rGO1, PS-rGO2, PS-rGO4, PS-FrGO1, PS-FrGO2 and PS-FrGO4) in four different types of oils

with those of PS-CNTs sorbents reported by Wu et al. [21], for sunflower oil, peanut oil, and motor oils which were 116, 123, and 112 g/g, respectively. Hence produced composite shows significant improvements in oil sorption is over those of commercially available non-woven polypropylene sorbent.

3.11 Oil sorption kinetics

Mechanism and rate of oil sorption on PS and PS-FrGOs sorbents were studied by three kinetic adsorption models, which are pseudo-first-order model (PFO), pseudo-second-order model (PSO), and intra-particle diffusion (IPD) model. Fitness of the models with experimental data was assessed by the coefficient of linear regression, R square (R^2) values and percentage Sum of Error Squares (SSE, %) which were computed and reported on Tables 4. Apart from R^2 values, applicability of PFO and PSO kinetic models were further assessed by the Sum of Error Squares.

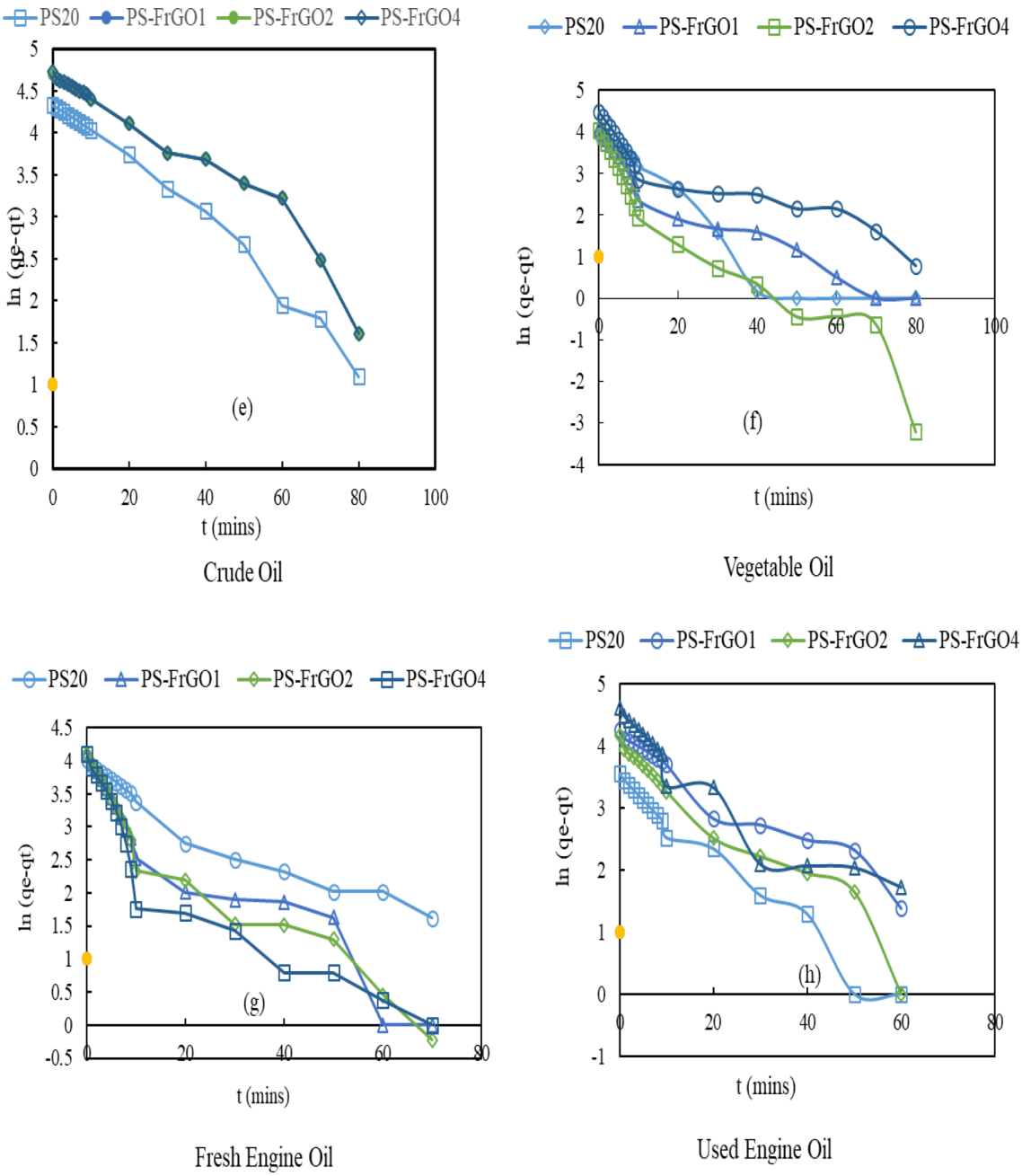

Fig. 10 Adsorption of four different types of oils with PS_{20}, PS-rGO_1, PS-rGO_2, PS-rGO_4, PS-$FrGO_1$, PS-$FrGO_2$ and PS-$FrGO_4$ based on Pseudo first order (PFO) kinetics

(SSE, %). The closer the R^2 value is, to unity, and the lower the value of SSE, the better is the goodness of fit.

In this experiment, oily water mixture used was prepared by mixing 10 g of each oil samples in 150 ml distilled water. A known mass of electrospun PS and PS-FrGOs was allowed to float on the on the oily-water mixtures surface till the end of the sorption process. As shown in Fig. 9a, sorption of crude oil on PS and PS-FrGOs increased rapidly within the first 30 min, it slows down significantly in the next 50 min and attained equilibrium between (80 – 100) minutes. Similarly, vegetable oil, fresh engine oil and used engine oil sorption on the two sets of composites increase rapidly within the first 20 min, slows down within the next 30–60 min and had all attained equilibrium at 70–90 min, this is presented in Fig. 9b–d.

Figures 10e–h and 11 i–l present sorption of the four types of oils on the two sets of composites based on pseudo-first-order (PFO) and pseudo-second-order kinetic models (PSO). As shown on Tables 4, sorption of the four oil samples based

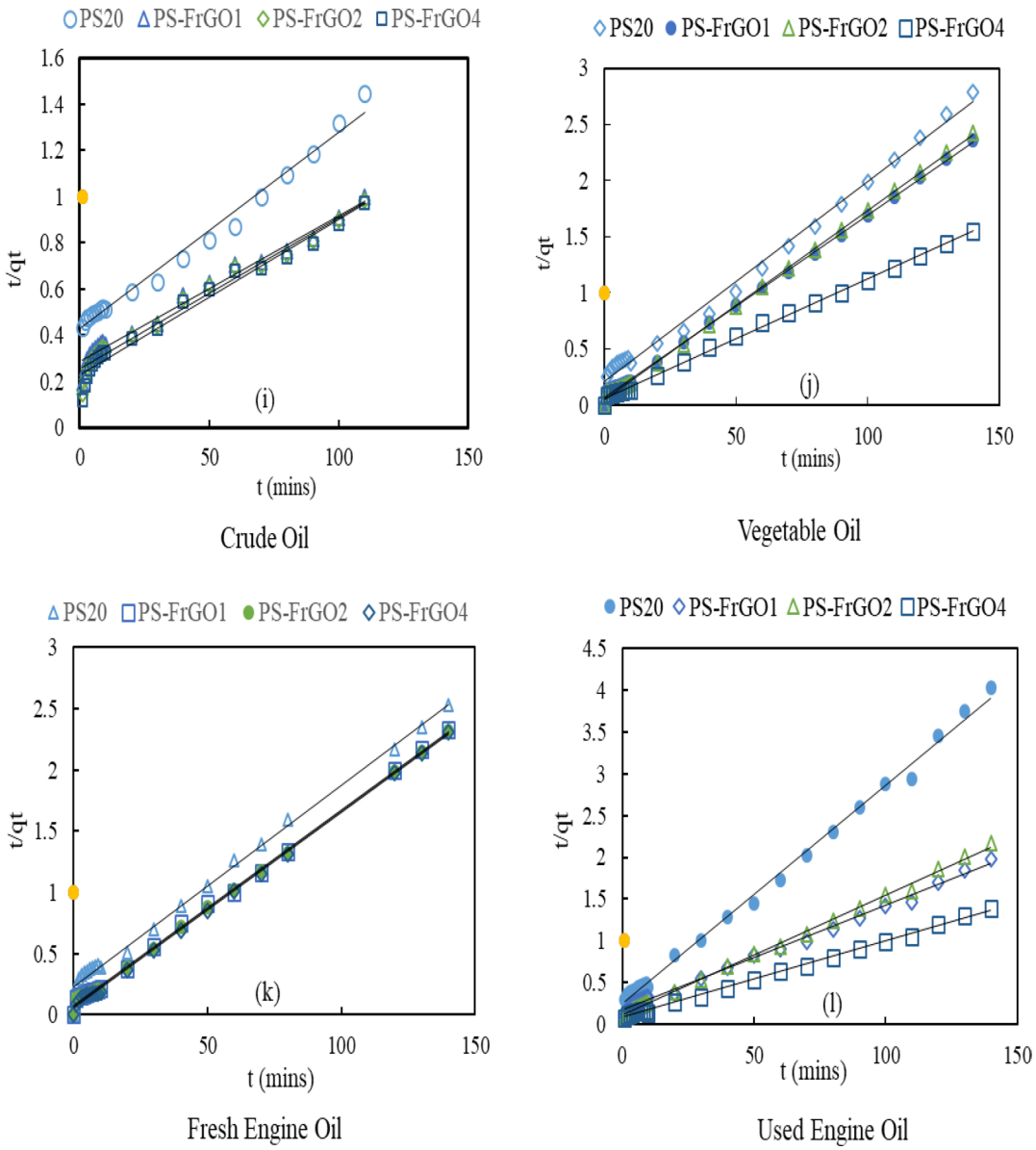

Fig. 11 Adsorption of four different types of oils with PS_{20}, PS-rGO_1, PS-rGO_2, PS-rGO_4, PS-$FrGO_1$, PS-$FrGO_2$ and PS-$FrGO_4$ based on Pseudo second order (PSO) kinetics

on pseudo-second-order kinetics fits the experimental data best with R^2 values closest to one (1), this result agrees with the reports of Wu et al. [21] and those of Lakayan et al. [32]. Figure 12 (m–p) show sorption of the four types of oils on the two sets of composites based on the intraparticle diffusion (IPD) model. This model shows that sorption of these oils on the seven composites is divided into three (3) Phases. At various loadings of FrGO on the polystyrene, for the sorption of each oils, IPD plots did not pass through the origin, hence producing a non-zero inter intercepts. The non-zero intercept obtained for all adsorbate-adsorbent interaction suggests that oil sorption rate is affected by multiple parameters such as viscosity, oil density, surface area, porosity, surface tension, and oleophilicity. Reports of Mookgo et al. [35] agrees with these results. For the sorption of the four oil samples considered, coefficient of linear regression, R square (R^2) values based on IPD model, shows a good fit with experimental data in the first and second oil sorption phases.

3.12 Reusability of PS_{20} and PS-FrGO composite as oil sorbents

Used PS-FrGO composites was compressed between two (2) flat plates and rinsed in ethanol and distilled water to investigate the reusability of PS-FrGO composites. After which they were dried in an oven at 60 ^{0}C for about 15 min. No

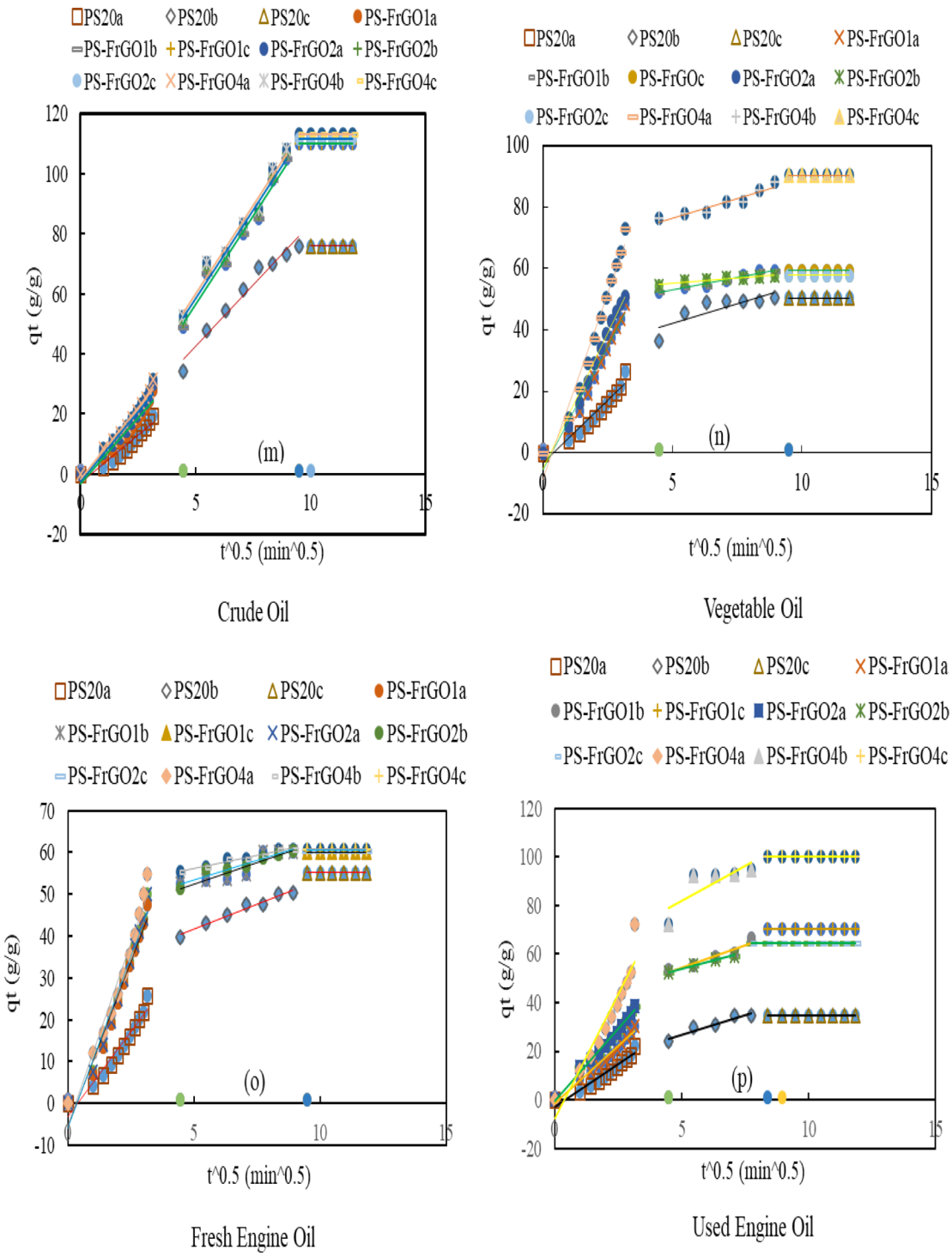

Fig. 12 Adsorption of four different types of oils with PS_{20}, PS-rGO_1, PS-rGO_2, PS-rGO_4, PS-$FrGO_1$, PS-$FrGO_2$ and PS-$FrGO_4$ based on Intraprticle Diffusion (IPD) model kinetics

structural collapse was observed in the PS-FrGO composites, although a sharp decrease in oil removal rate was observed in all composites, after the second all adsorption cycle. However, in the second sorption/desorption cycle, PS-$FrGO_1$, PS-$FrGO_2$ and PS-$FrGO_4$ have significantly high oil adsorption capacity in motor oil. Reusability of three composites sorbent in four oil samples during three oil sorption–desorption cycles is shown in Fig. 13.

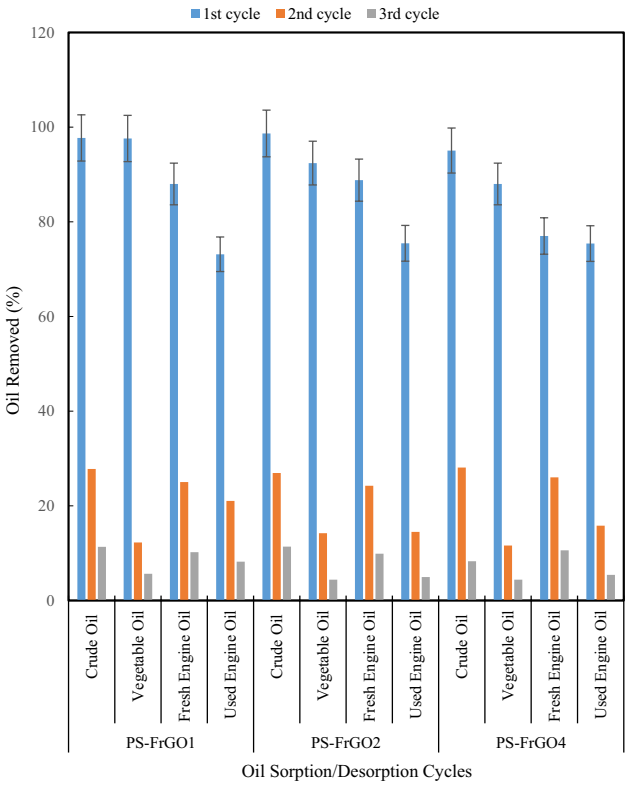

Fig. 13 Oil removal efficiency of composite sorbents in three sorption cycles

4 Conclusion

Surface modified rGO with hydrophobic functional groups, 0.0729 cm^3/g pore volumes and 156.36 m^2/g surface area was synthesized. When the synthesized FrGO was infused in PS, highly hydrophobic PS-FrGO composite sorbents was successfully fabricated. Pure PS has a pore volume 0.0252 cm^3/g and specific surface area 71.52 m^2/g. Infusion of FrGO in PS, produced composites with surface area significantly higher than those of pure PS, for instance; 456.143 m^2/g for PS-$FrGO_4$. The composites were tested for oil sorption, and pure PS shows sorption capacity 46.32 g/g in crude, while PS-$FrGO_4$ showed 168.83 g/g. Surface area and adsorption capacities, of produced composites are larger than those reported by Wu et al. [21] as well as Lakayan et al. [32]. Linear correlation coefficient (R^2) value, confirms that PSO Kinetic model best fits adsorption of the four oil samples on the four composite sorbents produced. As evident from the IPD model, sorption of the four oil samples on the four composite sorbents, occurred in three (3) phases. The three composites show good recyclability in the four oil samples, at least up to the third sorption cycle.

Acknowledgements Supports received from the Nanomaterial Industrial Development Facility, of DST-CSIR Nanotechnology Innovation Centre, of the Department of Science and Technology, Pretoria, Republic of South Africa, are highly acknowledged.

Author contributions I. O. A., B.Y.J. and M. O. D., Conceptualization; I. O. A. and S. A. I., Data Curation; I. O. A., Formal Analysis; B. Y. J., M. O. D. and I. O. A, Funding acquisition; S. A. I. and I. O. A., Investigation; S. A. I. and I. O. A., Methodology; B. Y. J. and M. O. D., Project administration; M. O. D. and I. O. A., Resources; B. Y. J., M. O. D. and I. O. A., Software; B. Y.J., M. O. D., B. S. S., B. M. and S. A. I., Supervision; B. S. S., B. M. and I. O. A., Validation; B. S. S. and B. M., Visualization; I. O. A., Writing—Original Draft; B. Y. J., B. M., B. S. S., S. A. I., M.O.D. Writing—Review & Editing. All authors reviewed the manuscript.

Funding This research work was supported by Petroleum Technology Development Fund (PTDF/ED/LSS/PHD/AOI/0368/19), (PTDF), Abuja, as well as PTDF Chair in Chemical Engineering of Ahmadu Bello University, Zaria, Nigeria. However, the sponsors are not in any way involved in the experimental design; data collection/analysis and interpretation, nor in writing of this manuscript; and decision on where to publish the article.

Availability of data and material All data supporting the findings of this study are available within the paper.

Declarations

Competing interests The authors hereby declare that there are no known competing interests, financial or personal relationships, that could have appeared to influence works reported in this paper.

References

1. NOSDRA. *Nigerian Oil Spill Monitor.* 2023. https://oilspillmonitor.ng. Accessed 20th May, 2023.
2. Abdulhussein AT, Kannarpady GK, Ghosh A, Steiner RC, Mulon PY, Anderson DE, Biris AS. Facile fabrication of a free-standing superhydrophobic and superoleophilic carbon nanofiber-polymer block that effectively absorbs oils and chemical pollutants from water. Vacuum. 2018;149:39–47. https://doi.org/10.1016/j.vacuum.2017.11.028.
3. Santander M, Rodrigues RT, Rubio J. Modified jet flotation in oil (petroleum) emulsion/water separations. Colloids Surf, A. 2011;375:237–44.
4. Dalawai SP, Saad Aly MA, Latthe SS, Xing R, Sutar RS, Nagappan S. Recent advances in durability of superhydrophobic self-cleaning technology: a critical review. Progr Org Coat. 2020;138:105381. https://doi.org/10.1016/j.porgcoat.2019.105381.
5. Latthe SS, Kodag VS, Sutar RS, Bhosale AK, Nagappan S, Ha CS. Sawdust-based superhydrophobic pellets for efficient oil-water separation. Mater Chem Phys. 2020;243:122634. https://doi.org/10.1016/j.mtchemphys.2020.122634.
6. Luo Y, Wang X, Zhang R, Singh M, Ammar A, Cousins D, Hassan MK, Ponnamma D, Adham S, Al-Maadeed MA, Karim A. Vertically oriented nanoporous block copolymer membranes for separation and filtration. J Soft Matter. 2020;16:9648–54. https://doi.org/10.1039/D0SM00526F.
7. Sarbatly R, Krishnaiah D, Kamin Z. A review of polymer nanofibres by electrospinning and their application in oil–water separation for cleaning up marine oil spills. Mar Pollut Bull. 2016;106:8–16. https://doi.org/10.1016/j.marpolbul.2016.03.037.
8. Zadeh K, Luyt AS, Zarif L, Augustine R, Hasan A, Messori M, Hassan MK, Yalcin HC. Electrospun polylactic acid/date palm polyphenol extract nanofibres for tissue engineering applications. Emerg Mater. 2019;2:141–51. https://doi.org/10.1007/s42247-019-00042-8.
9. Saravanan A, Kumar PS, Vardhan KH, Jeevanantham S, Karishma SB, Yaashikaa PV. A review on systematic approach for microbial enhanced oil recovery technologies: opportunities and challenges. J Clean Prod. 2020;258:120777. https://doi.org/10.1016/j.jclepro.2020.120777.
10. Al-Majed AA, Adebayo AR, Hossain MEA. sustainable approach to controlling oil spills. J Environ Manage. 2012;113:213–27.
11. Schrader E. Remediation of floating, open water oil spills: Comparative efficacy of commercially available polypropylene sorbent booms. Environ Geol Water Sci. 1991;17:157–66.
12. Robert S. Oil spill response performance review of skimmers. ASTM Int. 1998;34:34.
13. ITOPF. Technical Information Paper on Disposal of Oil and Debris. The International Tanker Owners Pollution Federation Limited (ITOPF). 2018. https://www.itopf.org. Accessed 24th May, 2018).
14. Deschamps G, Herve C, Marie-Elisabeth B, Christophe B, Christian V. Oil removal from water by selective sorption on hydrophobic cotton fibers; Study of sorption properties and comparison with other cotton fiber-based sorbents. Environ Sci Technol. 2003;37:1013–5. https://doi.org/10.1021/es020061s.
15. Moura FC, Lago RM. Catalytic growth of carbon nanotubes and nanofibers on vermiculite to produce floatable hydrophobic "nanosponges" for oil spill remediation. Appl Cataly B Environ. 2009;90:436–40. https://doi.org/10.1016/j.apcatb.2009.04.003.
16. Ahmad MA, Eusoff MA, Adegoke KA, Bello OS. Sequestration of methylene blue dye from aqueous solution using microwave assisted dragon fruit peel as adsorbent. J Environ Technol Innov. 2021;24:101917. https://doi.org/10.1016/j.eti.2021.101917.
17. Sandeep NT, Rao GSS, Mathur AB, Jasra R. Polyolefin/graphene nanocomposites: a review. RSC Adv. 2017;7:23615–32. https://doi.org/10.1039/C6RA28392F.
18. Mohamadreza S, Majid A, Saeedeh M, Mohammad RK. Super-hydrophilic electrospun PAN nanofibrous membrane modified with alkaline treatment and ultrasonic-assisted PANI in-situ polymerization for highly efficient gravity-driven oil/water separation. J Sep Purif Technol. 2023;309: 123032. https://doi.org/10.1016/j.seppur.2022.123032.
19. Ibrahim K, Ebubekir SA. Electrospun PAN-PS membranes with improved hydrophobic properties for high-performance oil/water separation. J Separ Purif Technol. 2024;331:125590. https://doi.org/10.1016/j.seppur.2023.125590.
20. Jin-Yong H, Eun-Ho S, Sungyoul P, Ho SP. Highly-efficient and recyclable oil absorbing performance of functionalized graphene aerogel. Chem Eng J. 2015;269:229–35. https://doi.org/10.1016/j.cej.2015.01.066.
21. Wu. J., An AK., Guo J., Lee EJ., Farid MU. And Jeong S. CNTs reinforced superhydrophobic-oleophilic electrospun polystyrene oil sorbent for enhanced sorption capacity and reusability. *Chemical Engineering Journal.* 2017;**314**:526–536. https://doi.org/10.1016/j.cej.2016.12.010.
22. Shiva G, Alireza R, Mohammadtaghi S, Ghorban A, Saeid A, Ali P. Application of polystyrene nanofibers filled with sawdust as separator pads for separation of oil spills. J Process Saf Environ Protect. 2021;146:161–8. https://doi.org/10.1016/j.psep.2020.08.044.

23. Ahmad AL, Sumathi S, Hameed BH. Adsorption of residue oil from palm oil mill effluent using powder and flake chitosan: equilibrium and kinetic studies. J Water Res. 2005;39:2483–94. https://doi.org/10.1016/j.watres.2005.03.035.
24. Wang J, Zixing S, Jinchen F, Yu G, Jie Y, Guoxin H. Self-assembly of graphene into three-dimensional structures promoted by natural phenolic acids. J Mater Chem. 2012;22:22459. https://doi.org/10.1039/C2JM35024F.
25. Pin-Hsuan C., Min-Chun S., Pei-Di J., Ruei-Ci W. and Chen-Bin W. Graphene sponge as an efficient and recyclable oil sorbent. *4th International Conference on the Advancement of Materials and Nanotechnology (ICAMN IV 2016)* (030005:1 - 10). USA: AIP Publishing. 2017. 978–0–7354–1557–7. https://doi.org/10.1063/1.4999861
26. Ren RP, Li W, Lv YK, Robust A. Superhydrophobic graphene aerogel as a recyclable sorbent for oils and organic solvents at various temperatures. J Colloid Interface Sci. 2017;500:63–8. https://doi.org/10.1016/j.jcis.2017.01.071.
27. Faniyi IO, Fasakin O, Olofinjana B, Adekunle AS, Oluwasusi TV, Eleruja MA, Ajayi EOB. The comparative analyses of reduced graphene oxide (RGO) prepared via green, mild and chemical approaches. Springer Nat J Appl Sci. 2019;1:1181. https://doi.org/10.1007/s42452-019-1188-7.
28. Oribayo O, Xianshe F, Garry L, Rempel QP. Synthesis of lignin-based polyurethane/graphene oxide foam and its application as an absorbent for oil spill clean-ups and recovery. J Chem Eng. 2017;323:191–202. https://doi.org/10.1016/j.cej.2017.04.0541385-8947.
29. Hoai NT, Sang NN, Hoang TD. Thermal reduction of graphene-oxide-coated cotton for oil and organic solvent removal. J Mater Sci Eng B. 2016;216:10–5. https://doi.org/10.1016/j.mseb.2016.06.007.
30. Lin YZ, Lu-Bin Z, Shuai D, Zai-Dong S, Qing L, Yu-Ming Z. Facile synthesis of electrospun carbon nanofiber/graphene oxide composite aerogels for high efficiency oils absorption. J Environ Int. 2019;128:37–45. https://doi.org/10.1016/j.envint.2019.04.019.
31. Al Azab M, Alnaqbi YE, Greish M, Mohsin EJ, Elumalai A, Al B. Morphological variations of micro-nanofibrous sorbents prepared by electrospinning and their effects on the sorption of crude oil. J Environ Chem Eng. 2016;4:1850–61. https://doi.org/10.1016/j.jece.2016.02.030.
32. Lakayan S, Behroozsarand A, Samadi A, Sirousazar M. Electrospun Polystyrene/Cloisite 20A fiber for selective separation of oil from water surface. J Environ Chem Eng. 2020;8: 103775. https://doi.org/10.1016/j.jece.2020.103775.
33. Abeer A, Mina SK, Syed RI, Guangbiao X, Aneeba C, Weaam A. Polymer Bulletin. 2023;80:4949–64. https://doi.org/10.1007/s00289-022-04297-w.
34. Abeer A, Mina S, Yujie W, Andrew B, Mhd F, Shengyuan Y. Functionalization of aminoalkylsilane-grafted cotton for antibacterial, thermal, and wettability properties. RSC Adv. 2022;12:20906–18. https://doi.org/10.1039/d2ra03214g.
35. Mookgo M, Lebea NN, Leonardo G, Phillemon M, Shivan M. Edward NN Perflurooctyltriethoxy silane and carbon nanotubes-modified PVDF superoleophilic nanofibre membrane for oil-in-water adsorption and recovery. J Environ Chem Eng. 2020;8:104497. https://doi.org/10.1016/j.jece.2020.104497.
36. Abeer A, Weaam A, Ibrahim A, Ghrood A, Rasha A. Facile fabrication of polystyrene/lignin /OV-POSS nanocomposite monolith by thermally induced phase separation method for wastewater cleanup. Polym Bull. 2024;81:10081–118. https://doi.org/10.1007/s00289-024-05193-1.